Title	Coherent nonlinear scattering of energetic electrons in the process of whistler mode chorus generation
Author(s)	Hikishima, Mitsuru; Yagitani, S.; Omura, Y.; Nagano, I.
Citation	Journal of Geophysical Research A: Space Physics (2009), 114(10)
Issue Date	2009
URL	http://hdl.handle.net/2433/91258
Right	An edited version of this paper was published by AGU. Copyright (2009) American Geophysical Union.
Type	Journal Article
Textversion	author

Coherent nonlinear scattering of energetic electrons in the process of whistler-mode chorus generation

M. Hikishima,[1,2] S. Yagitani,[2] Y. Omura,[1] and I. Nagano[3]

M. Hikishima, Y. Omura, Research Institute for Sustainable Humanosphere, Kyoto University, Uji, Kyoto 611-0011, Japan. (hikishima@rish.kyoto-u.ac.jp; omura@rish.kyoto-u.ac.jp)

S. Yagitani, Graduate School of Natural Science and Technology, Kanazawa University, Kakuma-machi, Kanazawa 920-1192, Japan. (yagitani@reg.is.t.kanazawa-u.ac.jp)

I. Nagano, Kanazawa University, Kakuma-machi, Kanazawa 920-1192, Japan. (nagano@reg.is.t.kanazawa-u.ac.jp)

[1]Research Institute for Sustainable Humanosphere, Kyoto University, Kyoto, Japan.

[2]Graduate School of Natural Science and Technology, Kanazawa University, Kanazawa, Japan.

[3]Kanazawa University, Kanazawa, Japan.

Abstract. Cyclotron resonant wave-particle interaction of whistler-mode chorus emissions drives pitch angle scatterings of a wide range of energetic electrons in the magnetosphere. We study a coherent scattering process associated with generation of the whistler-mode rising chorus emissions near the geomagnetic equator in a self-consistent electromagnetic full-particle simulation. The simulation shows that coherent whistler-mode rising chorus emissions scatter energetic electrons very effectively through formation of an electromagnetic electron hole. The nonlinear interaction induces acceleration of resonant electrons trapped by the wave and deceleration of untrapped resonant electrons. When the frequency of a rising chorus element continuously increases in time from lower frequencies to higher frequencies, the parallel resonant velocity continuously decreases toward lower velocity ranges resulting in significant scattering of resonant electrons. The lower limit of resonant parallel velocity is determined by the upper frequency limit of the rising chorus element. The unscattered electrons with low parallel velocities and the accelerated resonant electrons trapped by the wave result in the distribution clearly peaked at 90°. Successive generation of rising chorus elements can scatter resonant electrons in the same resonance velocity range. The repeated scatterings make the distribution much sharper at 90°, leading to formation of a pancake distribution function as observed in the inner magnetosphere.

1. Introduction

Chorus emissions are intense whistler-mode waves propagating along the ambient magnetic field line in the magnetosphere as reported by many observations [e.g., *Oliven and Gurnett*, 1968; *Burtis and Helliwell*, 1969; *Lauben et al.*, 1998; *Gurnett et al.*, 2001; *Meredith et al.*, 2001]. Generations of the chorus emissions are associated with injections of anisotropic energetic electrons predominantly during the recovery phases of disturbed geomagnetic storms [*Meredith et al.*, 2002a]. The generation region of the chorus emissions is restricted near the magnetic equator [*Tsurutani and Smith*, 1974, 1977; *Santolik et al.*, 2003, 2004a], and they propagate toward higher latitudes away from the equator [*Nagano et al.*, 1996; *LeDocq et al.*, 1998]. It is generally considered that chorus emissions are excited through nonlinear wave-particle interaction between anisotropic energetic electrons from several keV to tens of keV. The chorus emissions consist of various types of discrete elements, mainly rising tones which have steep increasing frequency variations with time, up to several tens of kHz/s [*Santolik et al.*, 2003, 2004a], and falling tones which are less frequently observed. Rising chorus emissions often appear in two distinct frequency ranges, the lower-band and upper-band with a gap at half the electron gyrofrequency, especially near the magnetic equator [*Tsurutani and Smith*, 1974; *Santolik et al.*, 2003, 2004b].

The quasi-linear diffusion theory has been used to account for the pitch angle scattering of magnetospheric electrons by the whistler-mode waves [*Lyons et al.*, 1971, 1972; *Horne et al.*, 2003b, 2005]. However, particle trapping and nonlinear effects have not been considered. *Horne et al.* [2005] have evaluated the pitch angle diffusion associated with assumed whistler-mode chorus in a wide energy range of electrons from tens of keV to MeV. The scatterings of resonant electrons at lower energies of tens of keV and at smaller pitch angles are dominant, and they are effectively precipitated into a loss cone. The ratio of the plasma frequency to the electron gyrofrequency in the magnetosphere can be a sensitive factor for the resonating energy range. In the lower plasma frequency region, the resonant diffusion of electrons in the higher energy range is dominant [*Summers et al.*, 1998].

Through the resonant interaction with whistler-mode waves, the resonant electrons diffuse in the direction to lower density regions depending on the density gradient in phase space [*Meredith et al.*, 2002b; *Horne and Thorne*, 2003], along the characteristic diffusion curve [*Kennel and Engelmann*, 1966]. As a result of the pitch angle diffusion, the gradients of the distribution function tend to approach to the diffusion curves [*Meredith et al.*, 1999]. Near the loss cone with small pitch angles, the diffusion of electrons is dominant due to the excessive depletion of electrons, which contributes to wave growth. *Brice* [1964] has argued the relationships between gain/loss of particle energy and wave damping/amplification. Additionally, *Gendrin* [1968, 1981] has considered different particle distribution functions including the loss cone distributions in detail. Under the consideration of density diffusion, the density gradient of the distribution function determines growth or damping of the waves.

Meredith et al. [1999] have reported the observations of characteristic distributions in the restricted region at the equator outside the plasmapause, where the pitch angle distributions are formed with sharply peaked at 90° in the relatively low energy range below a few keV, which is known as a pancake distribution [*Wrenn et al.*, 1979]. Similar types of pitch angle distributions in keV combined with butterfly distributions were reported [*Åsnes et al.*, 2005]. It has been suggested that ECH (Electron Cyclotron Harmonic) waves are responsible for the formation of pancake distributions [*Meredith et al.*, 2000]. *Horne et al.* [2003a] have shown that pitch angle distributions in the high energy range between a few hundred keV and a few MeV are observed during low frequency whistler-mode chorus emissions. The temporal variations of observed pitch angle distribution showed that the pancake distribution which peaks at 90° is dominated in energies of a few hundred keV during the recovery phase. They also described that the formation of the pancake distribution at ∼10 keV may be due to unscattered energetic electrons near 90°.

We have reproduced the generation process of whistle-mode rising chorus based on non-linear wave growth near the geomagnetic equator in a simulation [*Hikishima et al.*, 2009]. The simulation is carried out by an electromagnetic full particle simulation (KEMPO code) with a one-dimensional system [*Omura*, 2007]. Under the one-dimensional model with a cylindrical geometry of the ambient dipole magnetic field, we can only treat whistler-mode waves propagating parallel to the magnetic field. This may well be justified because the linear growth rate of whistler-mode waves maximizes in the parallel direction, and thus the wave can attain a sufficiently large wave amplitude leading to the nonlinear wave growth of chorus elements.

The particle simulation code can solve self-consistently the dynamics of full particle kinetics involving wave-particle interactions in the magnetosphere. Although the numerical simulations for chorus generation were performed in the past study [*Nunn et al.*, 1997; *Katoh and Omura*, 2007], the development of electron distribution associated with the interaction with chorus emissions has not been examined. In the present study, we show that there exist two different nonlinear scattering processes of energetic electrons associated with resonant interaction with whistler-mode chorus emissions in a self-consistent particle simulation.

2. Simulation Model

Maxwell's equations and equations of relativistic particle motion are self-consistently solved in the simulation. The particle simulation scheme, parameters, and the model are described by *Hikishima et al.* [2009]. We assume a one-dimensional system with a distance x taken along the static dipole magnetic field line near the geomagnetic equator. The dipole magnetic field is approximated by $B_{0x} = B_{0eq}(1 + ax^2)$, where B_{0eq} is a value at the equator. We assume the coefficient $a = 5.1 \times 10^{-6}\,\Omega_{e0}^2/c^2$, where Ω_{e0} is the electron gyrofrequency at the equator, and c is the speed of light. As plasma particles in the simulation, we use two species of particles, cold thermal electrons with an isotropic Maxwellian and energetic hot electrons with an anisotropic modified-Maxwellian for the loss cone. The loss cone distribution function of the energetic hot electrons in the relativistic momentum space $(u_\parallel, u_\perp)$ is realized by the following formula,

$$f(u_\parallel, u_\perp) = \frac{n_h}{(2\pi)^{3/2} U_{th\parallel} U_{th\perp}^2} \exp\left(-\frac{u_\parallel^2}{2U_{th\parallel}^2}\right) \cdot \frac{1}{1-\beta}\left[\exp\left(-\frac{u_\perp^2}{2U_{th\perp}^2}\right) - \exp\left(-\frac{u_\perp^2}{2\beta U_{th\perp}^2}\right)\right], \tag{1}$$

where n_h is the density of energetic hot electrons, and $U_{th\parallel}$, $U_{th\perp}$ are parallel and perpendicular components of the thermal momentum, respectively, and β is the depth of the loss cone. The thermal parallel and perpendicular momenta for the energetic hot electrons are $U_{th\parallel} = 0.20\,c$, and $U_{th\perp} = 0.33\,c$, respectively. The thermal momenta of energetic hot electrons realize a temperature anisotropy A ($= T_\perp/T_\| - 1$) ~ 2, where $T_\|$ and $T_\perp$ are parallel and perpendicular temperatures, respectively. The cold plasma frequency of electrons is assumed to be constant $\omega_{pe} = 5\,\Omega_{e0}$ along the magnetic field line.

3. Relativistic Resonance Curve

We assume an electron with the charge -e and the rest mass m_0 moving with a parallel velocity $v_\|$ and a perpendicular velocity $v_\perp$. A relativistic electron undergoes a gyromotion with a frequency Ω_e/γ, where Ω_e is the nonrelativistic electron gyrofrequency $\Omega_e = eB_{0x}/m_0$ and $\gamma = [1 - (v_\|^2 + v_\perp^2)/c^2]^{-1/2}$. In the presence of a whistler-mode wave with a frequency ω and a wavenumber k, the electron sees a constant wave phase when the following cyclotron resonance condition is satisfied,

$$\omega - kv_\| = \frac{\Omega_e}{\gamma} \ . \tag{2}$$

Taking the resonance condition $v_\| = V_R$, we simply obtain the relativistic resonance ellipse [*Summers et al.*, 1998],

$$V_R = c\delta\xi \left[1 - \frac{\Omega_e}{\omega} \left(1 - \frac{V_R^2 + v_\perp^2}{c^2} \right)^{1/2} \right] \ , \tag{3}$$

where we have eliminated the wavenumber k by defining dimensionless parameters ξ and δ which satisfy the cold plasma dispersion relation [*Omura et al.*, 2007, 2008],

$$\xi^2 = \frac{\omega\,(\Omega_e - \omega)}{\omega_{pe}^2} \tag{4}$$

and

$$\delta^2 = \frac{1}{1+\xi^2}\ . \tag{5}$$

Figure 1 shows the resonance curves for $\omega = 0.1,\ 0.3,\ 0.5,\ 0.7\,\Omega_{e0}$ in the range of representative whistler-mode chorus wave frequencies in the velocity space. The velocity distribution function is that of the energetic electrons near the equator at the initial time $t = 0\,\Omega_{e0}^{-1}$ in the simulation. The lack of energetic electrons at lower pitch angles represents a relatively weak loss cone.

In the simulation, it should be noted that the relativistic energetic electrons with high energy MeV have low density in the tail of velocity distribution function. Two resonance curves at each frequency ω correspond to whistler-mode waves propagating with positive and negative k vectors (i.e., northward and southward propagating waves), interacting with counter-streaming electrons. The resonance curves can cross over the $v_\parallel = 0$ under a relativistic condition, and the parallel velocity $v_\parallel$ has the phase velocity $V_p = \omega/k = c\delta\xi$ at $v = c$.

4. Pitch Angle Scattering by Whistler-Mode Chorus

We consider electrons in resonance with a whistler-mode rising chorus element in the magnetosphere. We give the schematic illustrations of a frequency-time spectrum of a typical rising chorus element, and examples of the resonance curves corresponding to different frequencies of the whistler-mode wave with positive k vectors in velocity space in Figure 2. The rising chorus element varies smoothly in frequency and wavenumber gradually increasing with time as A, B, and C in Figure 2a. The resonance curves A, B, and C corresponding to the three instantaneous frequencies are shown in Figure 2b. As the frequency of a chorus element varies from a low frequency to a higher frequency, the resonance curve shifts from a high parallel velocity region to a lower parallel velocity region of the distribution function of energetic electrons. When chorus elements are observed with both positive and negative k vectors near the equator [*Santolik et al.*, 2003], the development of the electron distribution by resonance curves takes place in both positive and negative $v_{\|}$ regions of the velocity space.

We have shown generations of whistler-mode rising chorus wave packets near the geomagnetic equator [*Hikishima et al.*, 2009]. The rising chorus wave packets are excited all over the simulation system corresponding to the equatorial region and then propagate toward higher latitude regions in both hemispheres, i.e., northward ($+x$ direction) and southward ($-x$ direction). Therefore, the rising chorus emissions at fixed point near the equator are composed of wave packets having positive and negative k vectors and varying in frequency and amplitude. To evaluate counter-streaming resonant interactions, we need to know accurate amplitudes and frequency of a rising chorus element propagating to one direction. Hence, we separate the chorus wave packets propagating in both hemispheres into northward and southward propagating waves. This is realized by separating wavenumber modes on the frequency-wavenumber domain all over the simulation region. We apply the Fourier transform in space for transverse whistler-mode wave magnetic fields B_y, and B_z propagating in the simulation region. Then we apply the inverse Fourier transform for the separated modes after obtaining the desired wavenumber mode ($+k$ or $-k$). Thus, we obtain the whistler-mode wave packets propagating with positive k or negative k vector. In Figure 3a, we show the transverse wave magnetic field $B_w = (B_y^2 + B_z^2)^{1/2}$ of wave packets of rising chorus propagating northward (right panel) and southward (left panel), and Figure 3b shows the dynamic spectra at the equator for northward (upper panel) and southward (lower panel) propagating rising chorus wave packets. The colored squares are used in Figure 4.

In Figure 4, we show the temporal variation of the velocity distribution function of energetic electrons at the equator. The panels (i)∼(vi) correspond to timings $t = 0, 1310, 1640, 2290, 3280$, and $9994\,\Omega_{e0}^{-1}$ indicated in Figure 3b, respectively. It is noted that the contour scale of phase space density differs from that in Figure 1 for observation of fine structures of velocity distribution functions. The colored curves superimposed on the velocity distribution functions in (ii)∼(v) represent the resonance curves related to the rising chorus frequencies in the dynamic spectra in Figure 3b, and the resonance curves given in the positive and negative $v_\parallel$ regions on the velocity distribution functions correspond to southward and northward propagating waves, respectively. Each colored resonance curve corresponds to each colored square on the dynamic chorus spectra. In panel (i), dashed white semicircles superimposed on the distribution function indicate the constant kinetic energies of energetic electrons, $K = 1$, 10, 50, 100 keV, respectively.

At time (i) in Figure 4, we find the initial anisotropic distribution function of energetic electrons with loss cones. At time (ii), the lower frequency band approximately $\omega = 0.15 \sim 0.35\,\Omega_{e0}$ forms rising chorus, but still in an embryonic form. The energetic electrons at the equator encounter the enhanced wave packets of whistler-mode waves with the broad frequency band which are generated around the equator. The resonant electrons on the resonance curves (white curves) in the velocity space are strongly scattered in the wide parallel velocity range corresponding to the frequency band. We find the significant deformation along the resonance curves which are especially determined by the upper frequency limit of the excited waves (white square). At this time the resonance velocity are symmetry in $+v_{\parallel}$ and $-v_{\parallel}$ velocity regions because the excited wave packets with $+k$ and $-k$ vectors have almost the same frequency components. At time (iii), the resonant electrons interact with a higher frequency part of a rising chorus element, which leads to scattering in the lower parallel velocity region. Additionally, the deformation of velocity distribution function by another enhanced rising chorus element with a different frequency (blue) is seen. On the other hand, significant precipitation of energetic electrons into the loss cone region occurs because of relatively broadband waves at $\omega \sim 0.2\,\Omega_{e0}$. The loss cone regions are filled with a large number of scattered electrons. At time (iv), the resonance curves gradually shift to lower parallel velocity region. The higher frequency part of the rising chorus element continues to scatter electrons in the lower parallel velocity. At time (v), another low frequency chorus element (orange) appears, and resonant electrons in the higher velocity range are repeatedly scattered. Scattering of electrons at lower parallel velocity continues until the rising chorus frequency stops, where enhanced scattering is not seen since the chorus wave amplitude at the higher frequency (white) is relatively weak. At time (vi), there appears no enhanced whistler-mode chorus element because of relaxation of the anisotropy of energetic electrons by resonance interactions of the foregoing chorus elements, and the scattering of electrons at the equator stops. At this stage, the unscattered energetic electrons in the low energy range remain as the anisotropic distribution, while energetic electrons in the high energy range tend to form isotropic distribution as a result of repeated scattering by chorus elements [*Horne et al.*, 2003b]. On the other hand, we can see complete depletion of the scattered electrons inside the loss cone, which corresponds to the precipitations of the electrons into the ionosphere.

The temporal evolution of the velocity distribution functions during (i)∼(vi) shows clearly that even just a single whistler-mode chorus element can easily deform the original anisotropic distribution function by one sweep of resonance curve from a higher velocity to a lower velocity, which corresponds to a short period $t \sim 3000\,\Omega_{e0}^{-1}$. The deformation of the distribution function is more enhanced by successive excitation of chorus elements near the equator.

The resonance velocity widely changes in ($v_\parallel$, $v_\perp$) space, which is determined by a range of chorus frequency ω/Ω_{e0} and electron plasma frequency ω_{pe}/Ω_{e0}. The lower electron plasma frequency makes chorus emissions interact with the higher energy electrons [*Summers et al.*, 1998]. In the simulation, the resonance energy at small pitch angles corresponding to the loss cone regions varies from a few keV to tens of keV. On the other hand, the electrons can resonate in the wide energy range of more than hundreds of keV at larger pitch angles (see Figure 1).

5. Nonlinear Scattering of Resonant Electrons

The pitch angle scattering process described above is essentially different from the diffusion process as assumed in the quasi-linear diffusion theory. We show two types of nonlinear scattering processes corresponding to acceleration and deceleration of electrons in the followings.

During resonant interaction the electrons are trapped by the potential of whistler-mode wave. Figure 5 shows trajectories of resonant electrons in (θ, ζ) phase space for the condition of the inhomogeneity ratio $S = -0.41$ which is given by *Omura et al.* [2008, Figure 1], where $\theta = k(v_\parallel - V_R)$ and ζ is a phase angle between the transverse wave magnetic field and the perpendicular velocity of an electron. The trapping potential is formed around the resonance velocity V_R corresponding to the instantaneous chorus frequency. It is noted that the phase space is defined in a specific $v_\perp$ of particle. The trapping region is separated by distinct distributions of the trapped (white region) and untrapped (gray region) electrons. Since most of resonant electrons remain untrapped, there arises an electromagnetic electron hole inducing the resonant current which contributes to nonlinear wave growth of chorus emissions [*Omura et al.*, 2008]. We can obviously find the appearances of nonlinear electromagnetic electron hole on the resonance velocity as shown in the followings.

To estimate the extension of electromagnetic electron hole, we suppose the condition with the inhomogeneity ratio $S = -0.41$ where the resonant current J_E maximizes contributing to nonlinear wave growth of chorus emissions [*Omura et al.*, 2008]. The trapping potential most widely spreads at the equilibrium point which represents a stable phase angle ζ_0 for the rotating trapped electrons in the (θ, ζ) phase space. The second-order derivative of the phase angle ζ gives

$$
\begin{aligned}
\frac{\mathrm{d}^2\zeta}{\mathrm{d}t^2} &= k\frac{\mathrm{d}}{\mathrm{d}t}(v_\parallel - V_R) \\
&= \omega_{tr}^2(\sin\zeta + S)\,, \qquad (6)
\end{aligned}
$$

where the relativistic trapping frequency $\omega_{tr} = \omega_t \delta\gamma^{-1/2}$ is given by the nonrelativistic trapping frequency $\omega_t = (kv_\perp \Omega_w)^{1/2}$, and Ω_w is electron gyrofrequency related to magnetic wave amplitude. We give a equation of separatrix of electromagnetic electron hole by *Omura et al.* [2008, Equation (43)], as

$$\theta_s(\zeta) = \pm\omega_{tr}\sqrt{2\Big[\cos\zeta_1 - \cos\zeta + S(\zeta - \zeta_1)\Big]} \,. \tag{7}$$

The second order resonance condition $\mathrm{d}^2\zeta/\mathrm{d}t^2 = \mathrm{d}\theta/\mathrm{d}t = 0$ gives the phase angle ζ_1 satisfying $\sin\zeta + S = 0$. The inhomogeneity ratio $S = -0.41$ gives $\sin\zeta_1 = 0.41$. Then the phase angle ζ_0 at equilibrium point is given by $\zeta_0 = \pi - \zeta_1$. We obtain the trapping velocity at the equilibrium phase angle ζ_0 as given by

$$V_{tr} = \frac{|\theta_s(\zeta_0)|}{k} = \left\{2\frac{\delta^2 v_\perp \Omega_w}{k\gamma}\Big[\cos\zeta_1 - \cos\zeta_0 + S(\zeta_0 - \zeta_1)\Big]\right\}^{\frac{1}{2}}$$

$$\sim 1.3\left[\frac{c\delta^3\xi v_\perp \Omega_w}{\gamma\omega}\right]^{\frac{1}{2}} \,. \tag{8}$$

In Figure 6, we plot the trapping velocities (dashed magenta curves) around at the resonance velocities (solid magenta curves) superimposed on the velocity distribution function (ii) in Figure 4. The white lines indicate contour of the distribution function. The examples of diffusion curves for the wave frequency $\omega = 0.32\,\Omega_{e0}$ are also plotted as blue curves. The range of the trapping region is given by $V_R \pm V_{tr}$ with a specific $v_\perp$ in the parallel velocity direction. The resonance and trapping velocities in the negative and positive parallel velocity regions are determined by the highest frequency $\omega = 0.32\,\Omega_{e0}$ and the magnetic wave amplitude $B_w = 3.1 \times 10^{-3}\,B_{0eq}$ of the rising chorus element at time (ii). The parallel velocity of resonant electrons change within the range of $V_R \pm V_{tr}$. The trapping period is estimated by $T_{tr} = 1/\omega_{tr} \sim 18\,\Omega_{e0}^{-1}$ for resonant electrons at $v_\perp = 0.3\,c$. The electron hole and its trapping velocity are defined for a specific perpendicular velocity $v_\perp$ as indicated by (8). Averaged over the phase ζ, it appears as a depletion of the electron flux at the resonance velocity. The depletion along the resonance curve in Figure 6 represents an electron hole extended in the direction of $v_\perp$.

We focus on the nonlinear scattering process of the resonant electrons. Interacting with the rising chorus element, some of resonant electrons are trapped by the wave potential and rotate inside the electromagnetic electron hole in a presence of the nonlinear Lorentz force. The dynamics of electrons is given by equation of motion (6). With increasing frequency of a rising chorus element, the resonance velocity V_R decreases. The trapped electrons are guided to lower parallel velocity along decreasing resonance velocity. The trajectory of electrons follows the diffusion curve determined by a resonance frequency [*Gendrin*, 1981]. Therefore, since the trapped electrons are scattered to lower parallel velocity along the diffusion curve, the perpendicular velocity increases, being energized with increasing pitch angle along the diffusion curve. On the other hand, the untrapped resonant electrons rotate around the separatrix of the electromagnetic electron hole. The untrapped electrons flow in the direction in which the absolute parallel velocity increases (see Figure 5), i.e., in the direction of smaller pitch angle along the diffusion curve, giving energy to the chorus wave.

In Figure 7, we show the distributions of trapped electrons f_t and untrapped resonant electrons f_u in ($v_\parallel$, $v_\perp$) space. The electrons passing the equator ($x = -5 \sim +5\,c\Omega_{e0}^{-1}$) during the time $t = 1479 \sim 1525\,\Omega_{e0}^{-1}$ are counted. The trapped and untrapped electrons are identified by the increasing and decreasing of kinetic energy greater than 1keV. The electrons encounter a coherent rising chorus element with an increasing frequency $\omega = 0.33 \sim 0.37\,\Omega_{e0}$ during the short period. The trapped electrons (top left) oscillate around resonance velocity V_R corresponding to $\omega = 0.33\,\Omega_{e0}$ (black solid) in the range of the trapping region determined by the trapping velocity (black dashed). With the frequency increasing to $\omega = 0.37\,\Omega_{e0}$ at time $t = 1525\,\Omega_{e0}^{-1}$, the trapping region moves to a smaller $v_\parallel$ range shown in magenta. The motion of trapped electrons is recognized by shifting of the chain lines indicating the maximum density of the trapped electrons. On the other hand, the untrapped resonant electrons (top right) near the separatrix of the electromagnetic electron hole pass through the resonance velocity, flowing outside the separatrix. The movement of the untrapped resonant electrons results in an energy decrease by an amount greater than that of trapped electrons, and it is in the counter direction of trapped electron motion in $v_\parallel$ direction.

Trapped electrons is smaller compared with the untrapped electrons [*Katoh and Omura*, 2006]. The resonant current causing the nonlinear growth of chorus elements is predominantly due to the untrapped electrons. In Figure 8, we show the distribution functions $f(v_\parallel, v_\perp)$ and $f(v_\parallel, v_\perp = 0.3\,c)$ at the time (iii) in Figure 4. The depletion of electrons along the resonance velocity $v_\parallel \sim -0.15\,c$ obviously shows presence of an electromagnetic electron hole. The decelerated untrapped electrons form a hill of dense region next to the resonance velocity. Additionally, the electromagnetic electron holes at $v_\parallel \sim -0.26\,c$ are formed by a subsequent rising chorus element. These distinct nonlinear scatterings of trapped electrons and untrapped electrons result in the step-like distributions along the resonance curve in the phase space. It should be noted, however, these step-like distributions are different from those assumed by *Trakhtengerts* [1995]. The deformed distributions are due to formation of electron holes in the velocity phase space ($v_\parallel$, ζ).

6. Pitch Angle Distribution

We investigate the time evolution of the phase space density of energetic electrons as a function of pitch angle. We calculate the probability density function $f(v,\,\theta)$ of energetic electrons in the unit volume $\mathrm{d}v\mathrm{d}\theta$, where the velocity $v = (v_x^2 + v_y^2 + v_z^2)^{1/2}$ and the pitch angle θ. The probability density function $f(v,\,\theta)$ is obtained by dividing the particle number in a small volume $2\pi v^2 \sin\theta \mathrm{d}v\mathrm{d}\theta$ by the total number of particles over the three-dimensional velocity space.

To find time evolutions of the pitch angle distributions, we plot distributions of electrons with different kinetic energies $K = 50, 100, 200, 300$ keV in Figure 9. The panels (a)$\sim$(d) correspond to the times (i), (iii), (v), (vi) in Figure 4, respectively. Evaluating the phase space density, the energetic electrons within $\pm$ 5 % of each centered energy are counted in the region $x = -10 \sim +10\, c\Omega_{e0}^{-1}$ near the equator. In Figure 9a the purely anisotropic bi-Maxwellian distribution with relatively rounded is seen. The absence of electrons at small pitch angles over all energies is due to the loss cone and anisotropic distribution. In Figure 9b the resonant electrons are nonlinearly scattered along the diffusion curves, because of the increasing frequency of growing rising chorus element. The shapes of pith angle distribution are gradually deformed at higher pitch angles with increasing frequencies of rising chorus elements. The significant deformation of distribution function around $70^\circ \sim 80^\circ$ ($100^\circ \sim 110^\circ$) especially in energies K = 50, 100 keV are due to strong scattering of electrons on the resonance curves. The electrons in these energy range are possible to be scattered over almost all pitch angles except at the pitch angle near

90°. Unscattered electrons at the higher pitch angles in the lower energy remain to be bounced at the equator. During scattering by intensified rising chorus elements, a large number of untrapped electrons are precipitated into the loss cone. The scattering at small pitch angles in the range of $K = 50$ keV takes place dominantly, resulting in enhanced distributions of untrapped electrons in Figures 9b and 9c. In Figure 9c we also find that the electrons in the energy $K = 50$, 100 keV are scattered up to nearly 90° by higher frequency of rising chorus. Since other rising chorus elements subsequently appear, the number of scattered electrons falling into the loss cone increases further. After all the rising chorus elements propagate away from the equator, there occurs no scattering of electrons. In Figure 9d we find that all electrons inside loss cone are precipitated into the ionosphere.

The energetic electrons in the different energy ranges form pitch angle distributions especially peaked at 90°, which are called pancake distributions [*Wrenn et al.*, 1979; *Meredith et al.*, 1999; *Horne et al.*, 2003a]. The pancake distributions are formed below the energy of a few hundred keV. The pancake distributions consist of unscattered electrons from the initial state and resonant trapped electrons nonlinearly scattered to higher pitch angles. These electrons around 90° pitch angle continue to be bouncing near the equator. Rising chorus repeatedly generated near the equator can carry trapped resonant electrons to higher pitch angles while untrapped resonant electrons are effectively transferred to lower pitch angles. This could result in more enhanced pancake distributions.

At occurrence times of chorus emissions, pitch angle distributions of energetic electrons peaked at 90° are frequently observed [*Horne et al.*, 2003a; *Li et al.*, 2009]. *Horne et al.* [2003a] have investigated the pitch angle distributions in the energy ranges 0.15 $\sim$

1.58 MeV electrons during magnetic disturbances. The observed pitch angle distributions have shown the pancake distributions obviously peaked at 90° in energies of a few hundred keV. The pancake distributions we find in the present simulation agree very well with the observation results.

The pitch angle scattering involves two distinct nonlinear processes respectively for trapped and untrapped resonant electrons. The processes are due to interaction with a coherent wave, while the quasi-linear diffusion process assumes a spectrum of broadband waves with random phases. Therefore, it is not appropriate to describe the process in terms of the diffusion equation and a coefficient. A quantitative evaluation of the particle scattering by coherent chorus emissions was performed recently by *Furuya et al.*, [2008]. They used a numerical Green's function method to evaluate the effect of the nonlinear scattering based on test particle simulations.

We have reduced the size of the simulation system for numerical efficiency by assuming the large parabolic coefficient in the magnetic field variation. It has increased the threshold wave amplitude for the nonlinear growth as analyzed theoretically by *Omura et al.*, [2009]. The essential physical processes of acceleration and deceleration, however, are not changed, and the resulting pancake distribution near the equator should not be much different from the reality.

7. Summary

We have examined evolution of the velocity distribution functions of anisotropic energetic electrons by wave-particle interactions in the self-consistent electromagnetic full particle simulation. We summarize the simulation results as follows.

1. We have shown that the temporal developments of the distribution function of electrons by rising chorus emissions propagating parallel to the static magnetic field. This work is the first attempt to analyze the detailed scattering process of the resonant electrons by the chorus emissions.

2. It has been suggested that formation of electromagnetic electron holes is required for chorus emissions [*Omura et al.*, 2008, 2009]. We have found the depletion of resonant electrons correspond to the hole along the resonance curve. This clearly suggests the validity of the nonlinear wave growth theory for chorus emissions.

3. The resonant electrons dominantly undergo nonlinear scattering during the resonant interaction with rising chorus elements. The trapped electrons are accelerated to higher pitch angles while the untrapped resonant electrons are decelerated to lower pitch angles along the diffusion curve.

4. We have clarified formation process of the pancake distributions. It is formed by combination of unscattered electrons in the low energy and trapped resonant electrons. The whistler-mode chorus elements are successively generated while the unstable anisotropic distribution of energetic electrons is sustained. The electrons with pitch angles near 90° can exist stably near the equator. The peak of the distribution at 90° is efficiently enhanced by accumulating electrons accelerated by resonant wave trapping.

The rising chorus waves are formed with nonlinear wave growth near the magnetic equator, and grow as they propagate away from the equator [*Omura et al.*, 2008, 2009]. The resonant electrons are scattered by the chorus waves near the equator in the simulation. At a location far away from the magnetic equator, the resonance velocity becomes larger due to the increasing magnetic field intensity, and chorus waves cannot be generated because of insufficient flux of resonant electrons. Therefore, the effective scattering of resonant electrons is mostly caused in the vicinity of the magnetic equator.

We found a strong deformation of the velocity distribution function of energetic electrons in the simulation, which is a result of nonlinear coherent wave-particle interaction in the process of chorus generation. Since the time scale of a chorus element is of the order of a few hundred milliseconds in the Earth's magnetosphere, the progressive depletion of particle flux at the resonance curve would be confirmed by observation if a three-dimensional velocity distribution of energetic electrons in the $1 \sim 100$ keV range is obtained with a time scale of tens of milliseconds near the magnetic equator. This is a challenge to be made by future spacecraft observations.

Acknowledgments. Part of the computation in the present study was performed with the KDK system of RISH at Kyoto University. This work was partially supported by Grant-in-Aid 20340135 and 17GS0208 for Creative Scientific Research "The Basic Study of Space Weather Prediction" of the Ministry of Education, Science, Sports and Culture of Japan.

References

Åsnes, A., J. Stadsnes, R. W. H. Friedel, N. Østgaard, and M. Thomsen (2005), Medium energy pitch angle distribution during substorm injected electron clouds, *Geophys. Res. Lett.*, *32*, L10101, doi:10.1029/2004GL022008.

Brice, N. (1964), Fundamentals of VLF emission generation mechanisms, *J. Geophys. Res.*, *69*, 4515.

Burtis, W. J., and R. A. Helliwell (1969), Banded chorus – A new type of VLF radiation observed in the magnetosphere by OGO 1 and OGO 3, *J. Geophys. Res.*, *74*(11), 3002.

Furuya, N., Y. Omura, and D. Summers (2008), Relativistic turning acceleration of radiation belt electrons by whistler-mode chorus, *J. Geophys. Res.*, *113*, A04224, doi:10.1029/2007JA012478.

Gendrin, R. (1968), Pitch angle diffusion of low energy protons due to gyroresonant interaction with hydromagnetic waves, *J. Atmos. Terr. Phys.*, *30*, 1313.

Gendrin, R. (1981), General relationships between wave amplification and particle diffusion in a magnetoplasma, *Rev. Geophys.*, *19*, 171.

Gurnett, D. A., R. L. Huff, J. S. Pickett, A. M. Persoon, R. L. Mutel, I. W. Christopher, C. A. Kletzing, U. S. Inan, W. L. Martin, J.-L. Bougeret, H. St. C. Alleyne, and K. H. Yearby (2001), First results from the Cluster wideband plasma wave investigation, *Ann. Geophys.*, *19*, 1259.

Hikishima, M., S. Yagitani, Y. Omura, I. Nagano (2009), Full particle simulation of whistler-mode rising chorus emissions in the magnetosphere, *J. Geophys. Res.*, *114*, A01203, doi:10.1029/2008JA013625.

Horne, R. B., and R. M. Thorne (2003), Relativistic electron acceleration and precipitation during resonant interactions with whistler-mode chorus, *Geophys. Res. Lett.*, *30*(10), 1527, doi:10.1029/2003GL016973.

Horne, R. B., N. P. Meredith, R. M. Thorne, D. Heynderickx, R. H. A. Iles, and R. R. Anderson (2003a), Evolution of energetic electron pitch angle distributions during storm time electron acceleration to megaelectronvolt energies, *J. Geophys. Res.*, *108*(A1), 1016, doi:10.1029/2001JA009165.

Horne, R. B., S. A. Glauert, and R. M. Thorne (2003b), Resonant diffusion of radiation belt electrons by whistler mode chorus, *Geophys. Res. Lett.*, *30*(9), 1493, doi:10.1029/2003GL016963.

Horne, R. B., Richard M. Thorne, Sarah A. Glauert, Jay M. Albert, Nigel P. Meredith, and Roger R. Anderson (2005), Timescale for radiation belt electron acceleration by whistler mode chorus waves, *J. Geophys. Res.*, *110*, A03225, doi:10.1029/2004JA010811.

Katoh, Y., and Y. Omura (2006), A study of generation mechanism of VLF triggered emission by self-consistent particle code, *J. Geophys. Res.*, *111*, A12207, doi:10.1029/2006JA011704.

Katoh, Y., and Y. Omura (2007), Computer simulation of chorus wave generation in the Earth's inner magnetosphere, *Geophys. Res. Lett.*, *34*, L03102, doi:10.1029/2006GL028594.

Kennel, C. F., and F. Engelmann (1966), Velocity space diffusion from weak plasma turbulence in a magnetic field, *Phys. Fluids*, *9*, 12, 2377.

Lauben, D. S., U. S. Inan, T. F. Bell, D. L. Kirchner, G. B. Hospodarsky, and J. S. Pickett (1998), VLF chorus emissions observed by POLAR during the January 10, 1997, magnetic cloud, *Geophys. Res. Lett.*, *25*(15), 2995.

LeDocq, M. J., D. A. Gurnett, and G. B. Hospodarsky (1998), Chorus source locations from VLF Poynting flux measurements with the Polar spacecraft, *Geophys. Res. Lett.*, *25*(21), 4063.

Li, W., R. M. Thorne, V. Angelopoulos, J. W. Bonnell, J. P. McFadden, C. W. Carlson, O. LeContel, A. Roux, K. H. Glassmeier, and H. U. Auster (2009), Evaluation of whistler-mode chorus intensification on the nightside during an injection event observed on the THEMIS spacecraft, *J. Geophys. Res.*, *114*, A00C14, doi:10.1029/2008JA013554.

Lyons, L. R., R. M. Thorne, and C. F. Kennel (1971), Electron pitch-angle diffusion driven by oblique whistler-mode turbulence, *J. Plasma Phys.*, *6*, 589.

Lyons, L. R., R. M. Thorne, and C. F. Kennel (1972), Pitch-angle diffusion of radiation belt electrons within the plasmasphere, *J. Geophys. Res.*, *77*(19), 3455.

Meredith, N. P., A. D. Johnstone, S. Szita, R. B. Horne, and R. R. Anderson (1999), "Pancake" electron distributions in the outer radiation belts, *J. Geophys. Res.*, *104*(A6), 12,431.

Meredith, N. P., R. B. Horne, A. D. Johnstone, and R. R. Anderson (2000), The temporal evolution of electron distributions and associated wave activity following substorm injections in the inner magnetosphere, *J. Geophys. Res.*, *105*(A6), 12,907.

Meredith, N. P., R. B. Horne, and R. R. Anderson (2001), Substorm dependence of chorus amplitudes: Implications for the acceleration of electrons to relativistic energies, *J. Geophys. Res.*, *106*(A7), 13,165.

Meredith, N. P., R. B. Horne, R. H. A. Iles, R. M. Thorne, D. Heynderickx, and R. R. Anderson (2002a), Outer zone relativistic electron acceleration associated with substorm-enhanced whistler mode chorus, *J. Geophys. Res.*, *107*(A7), 1144, doi:10.1029/2001JA900146, 2002.

Meredith, N. P., R. B. Horne, D. Summers, R. M. Thorne, R. H. A. Iles, D. Heynderickx, and R. R. Anderson (2002b), Evidence for acceleration of outer zone electrons to relativistic energies by whistler mode chorus, *Ann. Geophys.*, *20*, 967.

Nagano, I., S. Yagitani, H. Kojima, and H. Matsumoto (1996), Analysis of wave normal and Poynting vectors of the chorus emissions observed by Geotail, *J. Geomag.*

Geoelectr., *48*, 299.

Nunn, D., Y. Omura, and H. Matsumoto, I. Nagano, and S. Yagitani (1997), The numerical simulation of VLF chorus and discrete emissions observed on the Geotail satellite using a Vlasov code, *J. Geophys. Res.*, *102*(A12), 27,083.

Oliven, M. N., and D. A. Gurnett (1968), Microburst phenomena, 3. An association between microbursts and VLF chorus, *J. Geophys. Res.*, *73*(7), 2355.

Omura, Y. (2007), One-dimensional electromagnetic particle code: KEMPO1, Advanced methods for space simulations, edited by H. Usui and Y. Omura, Terra Pub, pp.1-21.

Omura, Y., N. Furuya, D. Summers (2007), Relativistic turning acceleration of resonant electrons by coherent whistler mode waves in a dipole magnetic field, *J. Geophys. Res.*, *112*, A06236, doi:10.1029/2006JA012243.

Omura, Y., Y. Katoh, and D. Summers (2008), Theory and simulation of the generation of whistler-mode chorus, *J. Geophys. Res.*, *113*, A04223, doi:10.1029/2007JA012622.

Omura, Y., M. Hikishima, Y. Katoh, D. Summers, and S. Yagitani (2009), Nonlinear mechanisms of lower band and upper band VLF chorus emissions in the magnetosphere, *J. Geophys. Res.*, doi:10.1029/2009JA014206, *in press.*

Santolik, O., D. A. Gurnett, and J. S. Pickett (2003), Spatio-temporal structure of storm-time chorus, *J. Geophys. Res.*, *108*(A7), 1278, doi:10.1029/2002JA009791.

Santolik, O., D. A. Gurnett, and J. S. Pickett (2004a), A microscopic and nanoscopic view of storm-time chorus on 31 March 2001, *Geophys. Res. Lett.*, *31*, L02801, doi:10.1029/2003GL018757.

Santolik, O., D. A. Gurnett, and J. S. Pickett (2004b), Multipoint investigation of the source region of storm-time chorus, *Ann. Geophys.*, *22*, 2555.

Summers, D., Thorne, R. M., and Xiao, F. (1998), Relativistic theory of wave-particle resonant diffusion with application to electron acceleration in the magnetosphere, *J. Geophys. Res.*, *103*(A9), 20,487.

Trakhtengerts, V. Y. (1995), Magnetosphere cyclotron maser: BWO generation regime, *J. Geophys. Res.*, *100*(A9), 17,205.

Tsurutani, B. T., and E. J. Smith (1974), Postmidnight chorus: A substorm phenomenon, *J. Geophys. Res.*, *79*(1), 118.

Tsurutani, B. T., and E. J. Smith (1977), Two types of magnetospheric ELF chorus and their substorm dependences, *J. Geophys. Res.*, *82*(32), 5112.

Wrenn, G. L., J. F. E. Johnson, and J. J. Sojka (1979), Stable 'pancake' distributions of low energy electrons in the plasma trough, *Nature*, *279*, 5713,512.

Figure 1. Resonance curves with wave frequency $\omega = 0.1,\ 0.3,\ 0.5,\ 0.7\ \Omega_{e0}$ superimposed on the velocity distribution function of energetic electrons at the initial time $t = 0\,\Omega_{e0}^{-1}$ in the simulation.

Figure 2. Schematic illustration of a frequency variation of a typical rising chorus element (a), and variation of resonance curve (b) superimposed on the velocity distribution function $F(v)$ in the $(v_{\parallel},\ v_{\perp})$ space, and the dashed semicircle is curve of speed of light. Resonance curves A, B, and C in panel (b) correspond to different frequencies A, B, and C in panel (a), respectively.

Figure 3. (a) The transverse magnetic components of whistler-mode waves propagating toward northern (right panel) and southern (left panel) hemispheres. (b) Dynamic frequency spectra at the equator $x = 0\,c\Omega_{e0}^{-1}$ for the waves propagating toward the northern (upper panel) and southern (bottom panel) hemispheres. The colored squares correspond to the resonance curves in the same colors in Figure 4.

Figure 4. Velocity distribution functions of energetic electrons at the timings (i)∼(vi) in Figure 3b. The constant kinetic energy curves 1, 10, 50, 100 keV (dashed curves) are superimposed on the panel (i). The colored curves on the panels (ii)∼(v) indicate resonance velocities.

Figure 5. Trajectories of resonant electrons in the $(\theta,\ \zeta)$ phase space for the inhomogeneity ratio $S = -0.41$.

Figure 6. Trapping regions which are bounded by the trapping velocity (dashed magenta curves) around the resonance velocity (solid magenta curves), are plotted on the velocity distribution function (ii) in Figure 4. The blue curves indicate the diffusion curves.

Figure 7. Distributions of trapped and untrapped electrons at $t = 1479\,\Omega_{e0}^{-1}$ and $t = 1525\,\Omega_{e0}^{-1}$. The solid and dashed lines in black and magenta are resonance velocity and separatrix of the trapping region, respectively. The black lines are for $\omega = 0.33\ \Omega_{e0}$. The magenta lines are for $\omega = 0.37\ \Omega_{e0}$.

Figure 8. The distribution function $f(v_\parallel, v_\perp)$ at time (iii) in Figure 4 and its cross section at $v_\perp = 0.3\,c$.

Figure 9. Pitch angle distributions of electron phase space density with different kinetic energies $K = 50, 100, 200, 300$ keV. The panels (a)$\sim$(d) correspond to the times (i), (iii), (v), (vi) in Figure 4, respectively.

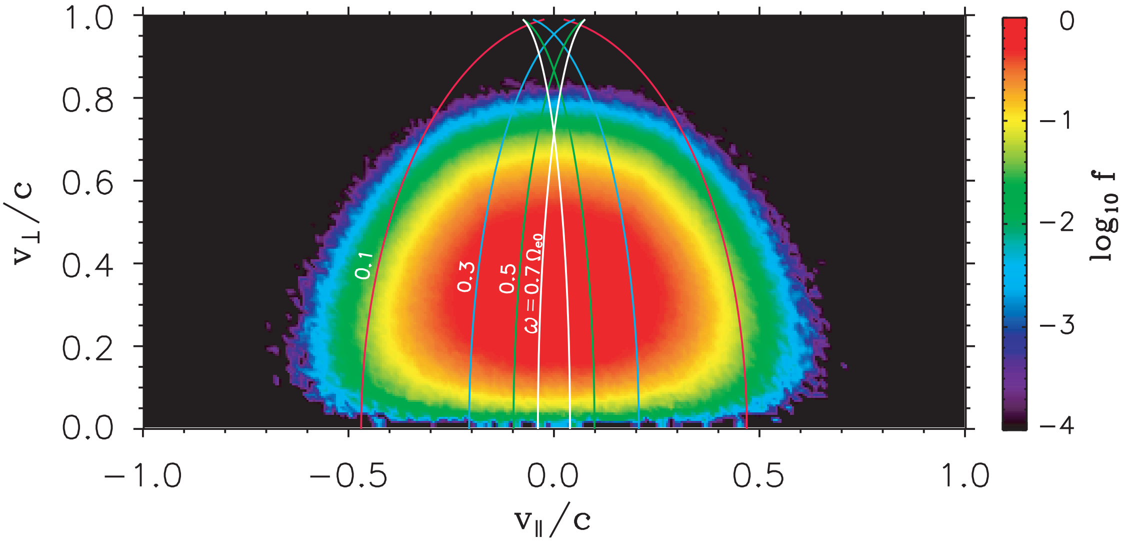

Figure 1. Resonance curves with wave frequency $\omega = 0.1,\ 0.3,\ 0.5,\ 0.7\ \Omega_{e0}$ superimposed on the velocity distribution function of energetic electrons at the initial time $t = 0\,\Omega_{e0}^{-1}$ in the simulation.

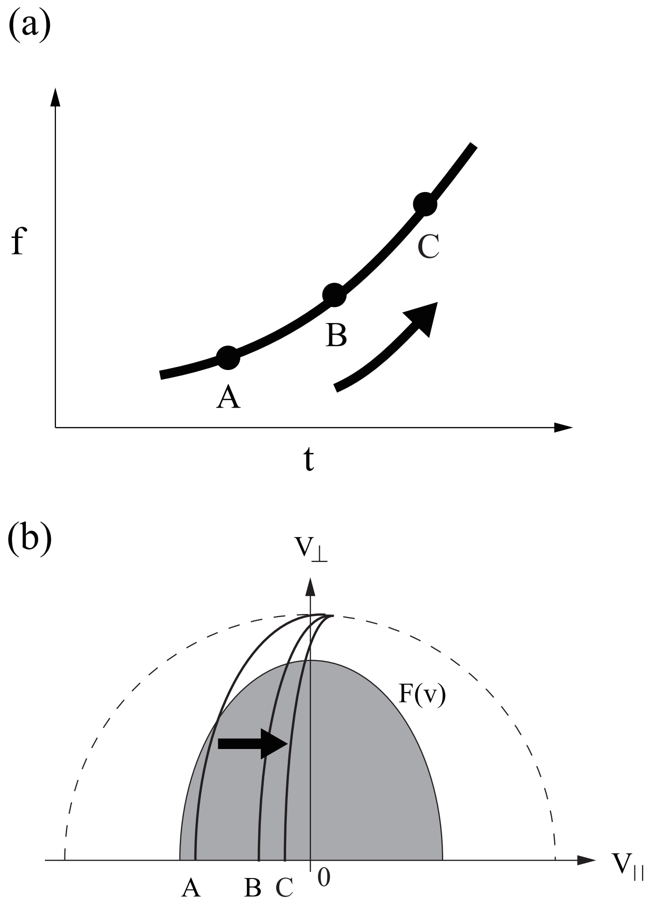

Figure 2. Schematic illustration of a frequency variation of a typical rising chorus element (a), and variation of resonance curve (b) superimposed on the velocity distribution function $F(v)$ in the $(v_{\|},\, v_{\perp})$ space, and the dashed semicircle is curve of speed of light. Resonance curves A, B, and C in panel (b) correspond to different frequencies A, B, and C in panel (a), respectively.

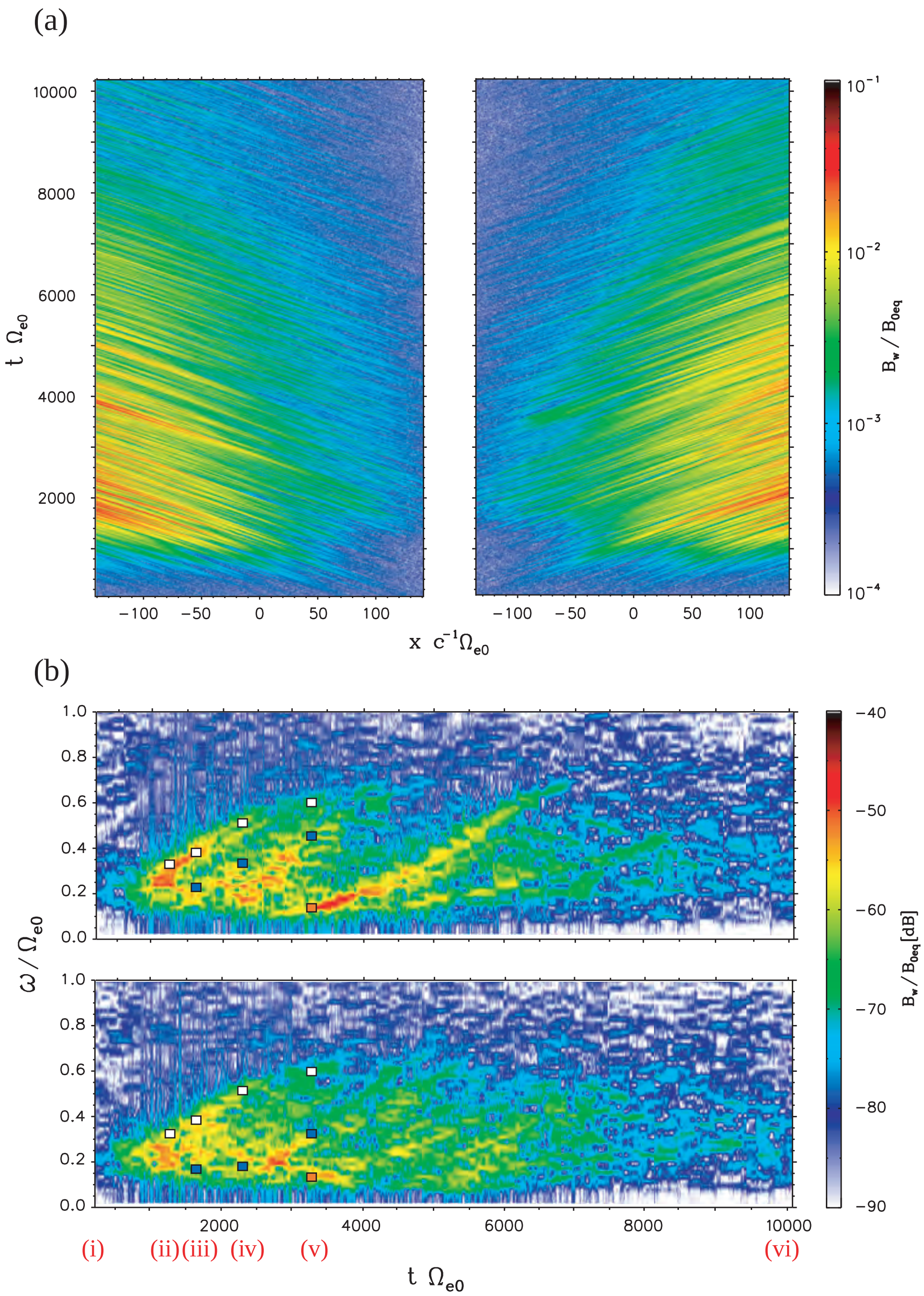

Figure 3. (a) The transverse magnetic components of whistler-mode waves propagating toward northern (right panel) and southern (left panel) hemispheres. (b) Dynamic frequency spectra at the equator $x = 0\, c\Omega_{e0}^{-1}$ for the waves propagating toward the northern (upper panel) and southern (bottom panel) hemispheres. The colored squares correspond to the resonance curves in the same colors in Figure 4.

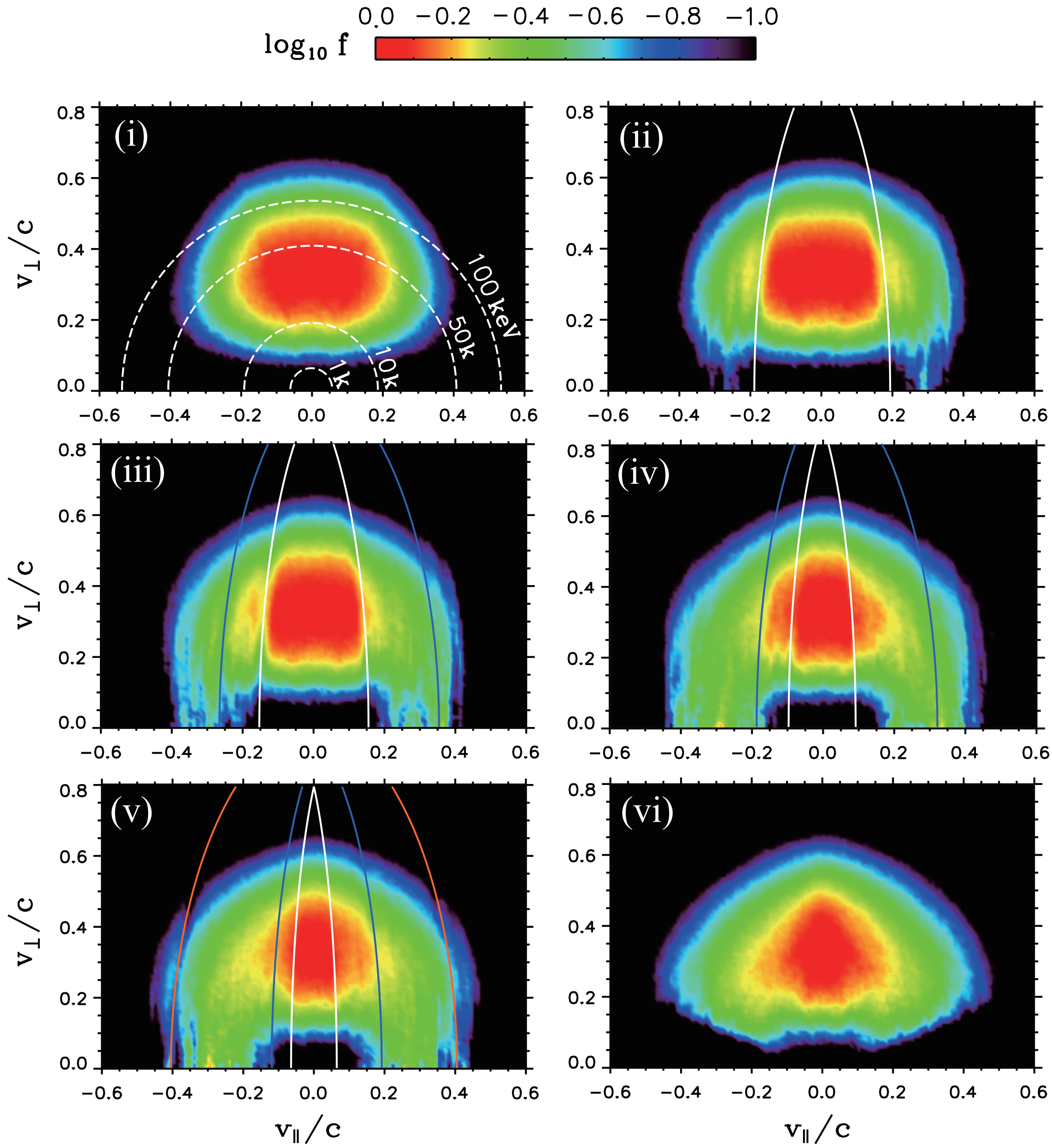

Figure 4. Velocity distribution functions of energetic electrons at the timings (i)∼(vi) in Figure 3b. The constant kinetic energy curves 1, 10, 50, 100 keV (dashed curves) are superimposed on the panel (i). The colored curves on the panels (ii)∼(v) indicate resonance velocities.

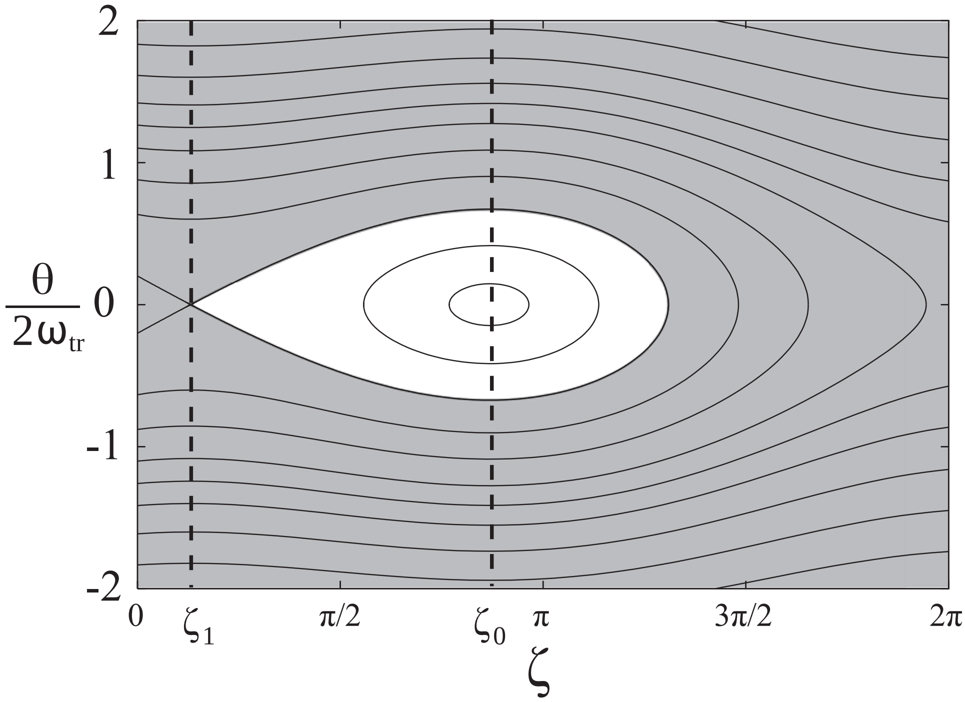

Figure 5. Trajectories of resonant electrons in the (θ, ζ) phase space for the inhomogeneity ratio $S = -0.41$.

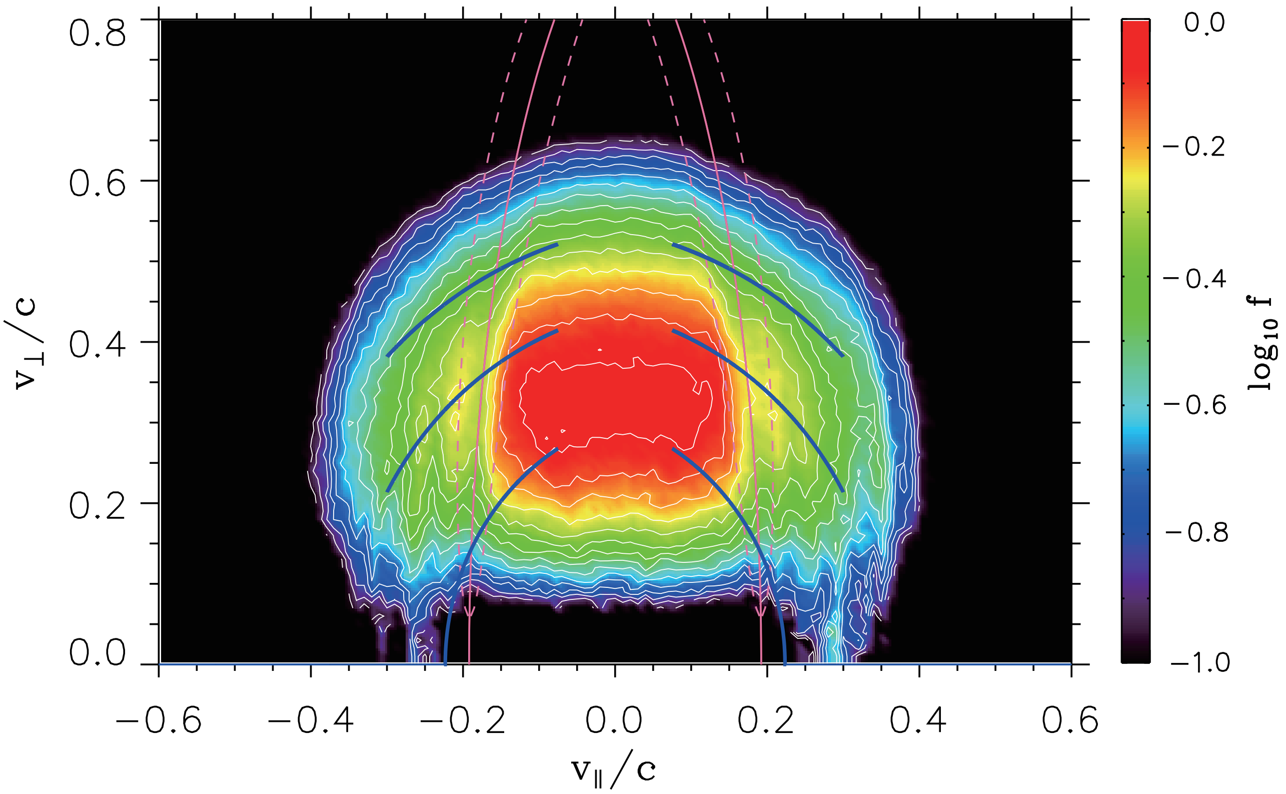

Figure 6. Trapping regions which are bounded by the trapping velocity (dashed magenta curves) around the resonance velocity (solid magenta curves), are plotted on the velocity distribution function (ii) in Figure 4. The blue curves indicate the diffusion curves.

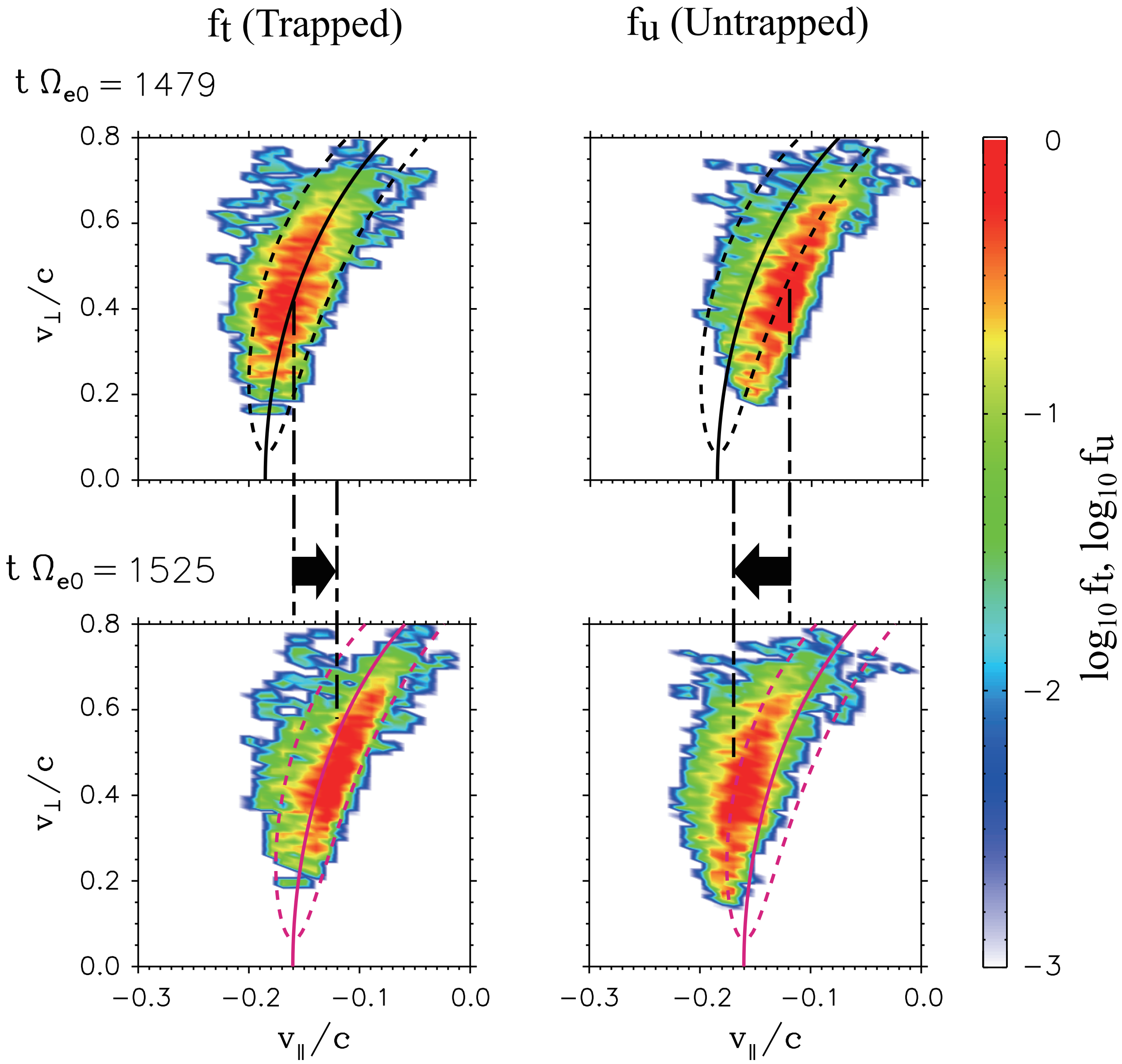

Figure 7. Distributions of trapped and untrapped electrons at $t = 1479\,\Omega_{e0}^{-1}$ and $t = 1525\,\Omega_{e0}^{-1}$. The solid and dashed lines in black and magenta are resonance velocity and separatrix of the trapping region, respectively. The black lines are for $\omega = 0.33\ \Omega_{e0}$. The magenta lines are for $\omega = 0.37\ \Omega_{e0}$.

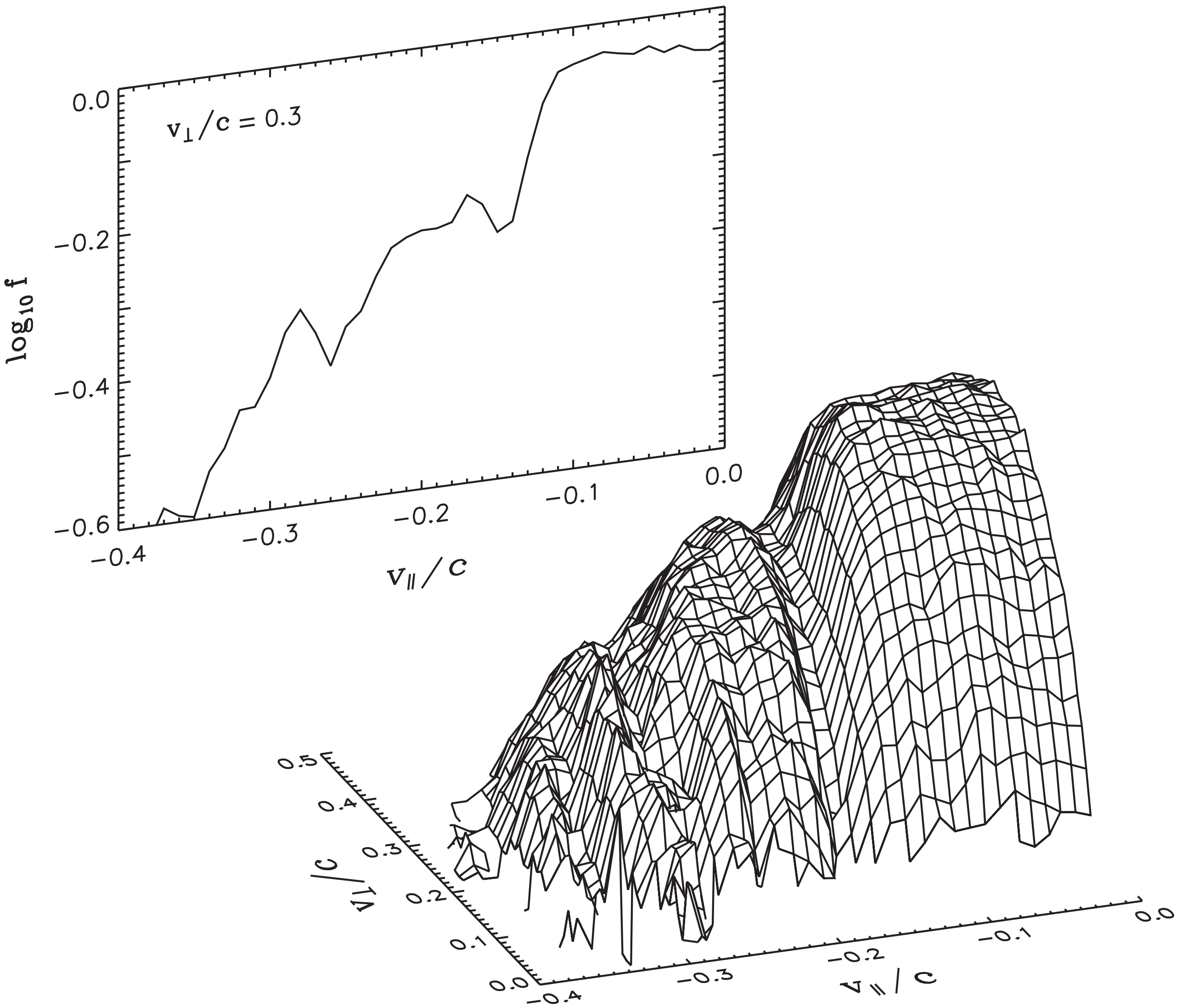

Figure 8. The distribution function $f(v_\parallel, v_\perp)$ at time (iii) in Figure 4 and its cross section at $v_\perp = 0.3\,c$.

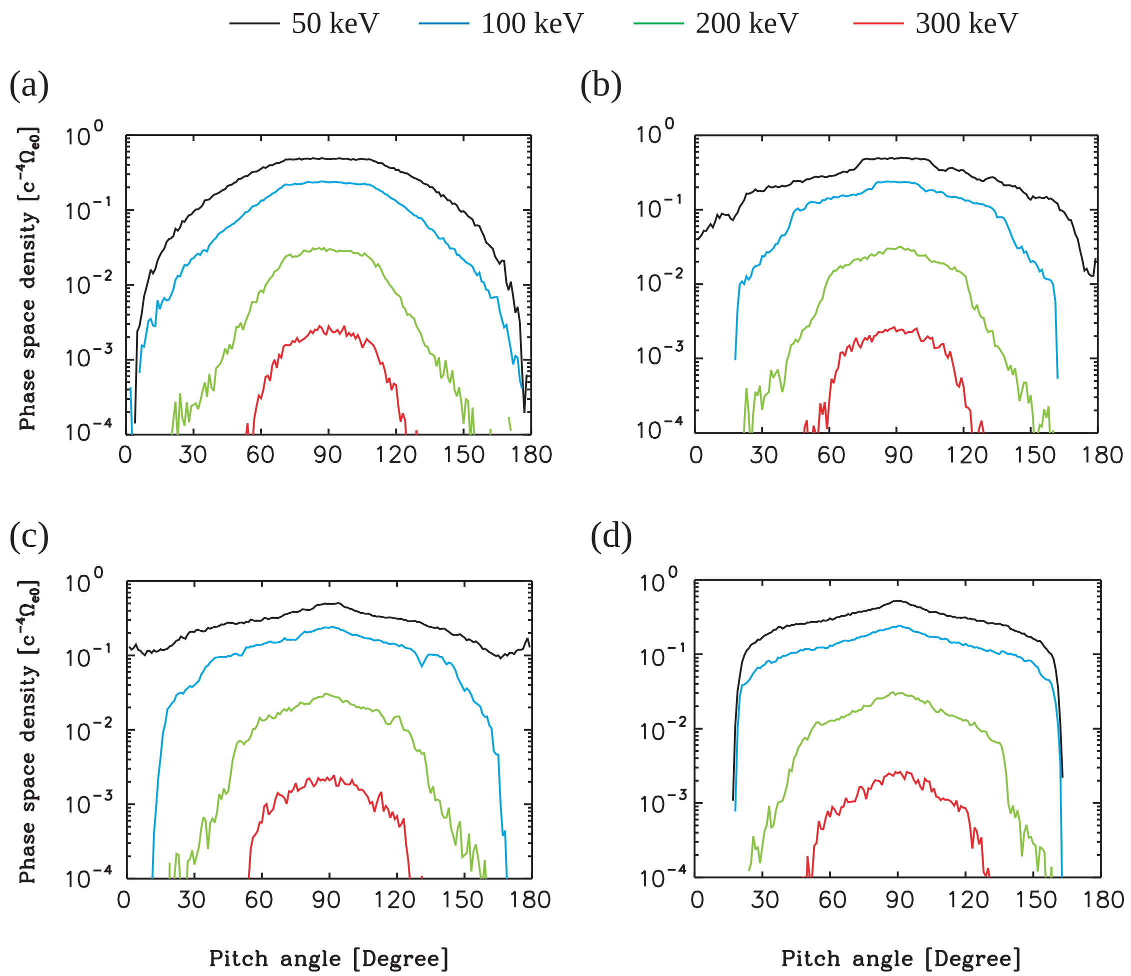

Figure 9. Pitch angle distributions of electron phase space density with different kinetic energies $K = 50, 100, 200, 300$ keV. The panels (a)$\sim$(d) correspond to the times (i), (iii), (v), (vi) in Figure 4, respectively.